Dalton Transactions

Accepted Manuscript






ROYAL SOCIETY OF CHEMISTRY

rsc.li/dalton

View Article Online
DOI: 10.1039/C8DT01787E

Journal Name

ARTICLE



# Nitrogen-doped Graphene-like Carbon Nanosheets from Commercial Glue: Morphology, Phase Evolution and Li-ion Battery Performance

Received 00th January 20xx,
Accepted 00th January 20xx

DOI: 10.1039/x0xx00000x

www.rsc.org/

D. Damodar,[a] S. Krishna Kumar,[b] S. K. Martha [b] and A. S. Deshpande*[a]

We report a two-step process to synthesize nitrogen-doped graphene-like carbon nanosheets (N-CNS), using commercially available ethyl cyanoacrylate based super glue as a carbon precursor. In this process, super glue is polymerized in aqueous NaCl solution, followed by carbonization at 1000 °C. The scanning electron microscopy (SEM) and high resolution transmission electron microscopy (HRTEM) studies show that the resultant material consists of micron-sized carbon nanosheets with wrinkled morphology. The HRTEM, X-ray diffraction (XRD), XPS and Raman spectroscopic studies confirm the formation of nanocrystalline and graphitic, nitrogen doped carbon nanosheets. Detailed FTIR analysis of the degradation products of the polymeric precursor (polyethyl cyanoacrylate) at various heat treatment temperatures in inert atmosphere reveals that, the polymer undergoes cyclization process similar to polyacrylonitrile (PAN) during carbonization to yield the N-CNS. The N-CNS used as an anode for lithium-ion battery shows stable reversible capacities of 480 mAh $g^{-1}$ for 100 cycles, which indicates that N-CNS are promising material for lithium-ion battery application. In a broader perspective, unique chemical transformation of polyethyl cyanoacrylate to graphitic carbon may be useful to design new nanostructured carbons for a plethora of applications.

## Introduction

The Nanostructured materials have generated immense interest in various advanced applications like energy storage, purification systems, electronic devices, sensors, actuators and bio-medical applications.[1-3] Various allotropes of carbon are commonly used active materials for these applications owing to their unique functional properties.[4-10] In particular, graphene and graphene-like two-dimensional nanosheets with $sp^2$ carbon network[11-16] possess fascinating properties, such as high electron mobility, electrical and thermal conductivity and Young's modulus. These attractive properties make them quite useful for various applications.[15,17,18] These properties can be further tailored by doping graphene with other elements such as B, N, P, and S and altering the size and shape of nanostructures.[19-22] Particularly, nitrogen doped carbon nanosheets (N-CNS) show significant changes in their functional behavior due to the presence of nitrogen in the form of pyridinic-N and pyrrolic-N groups within the hexagonal carbon network. The presence of such functional groups increases the affinity of the carbon material for adsorption of specific molecular moieties. As a result, the storage capacity of carbon nanostructures improves, which is desirable trait for various energy storage applications.[23] However, synthesis of nitrogen doped carbon nanosheets is still a challenging task. In general, synthesis of nitrogen doped carbon nanostructures can be categorized into two approaches, such as post-treatment method and *in-situ* synthesis method.[23] Post-treatment processes include direct thermal treatment of carbon nanosheets along with nitrogen containing precursors. These methods result in doping of nitrogen only on the surface and at edges of carbon nanosheets but not through the bulk of material.[23]

In contrast, *in situ* synthesis processes can yield carbon nanostructures with homogeneous incorporation of the dopant i.e. nitrogen substitution throughout the bulk of material. Moreover, usage of high quality carbon nanosheets as carbon source is not required. Thus, a wide variety of precursors can be used for the synthesis of N-CNS by *in situ* synthesis.[23] Using *in situ* process, high quality N-CNS can be produced. For example, N-CNS synthesized using chemical vapor deposition (CVD) is used in field-effect transistors, sensors and actuators.[23] However, CVD processes are expensive as ultra-high purity precursor gases are required for the growth of N-CNS. Furthermore, CVD is not suitable for applications such as lithium-ion batteries, super capacitors and hydrogen storage systems, where large quantities of N-CNS are required.[23] Apart from CVD, methods such as hydrothermal carbonization followed by chemical activation, segregation-

[a] Department of Materials Science and Metallurgical Engineering, Indian Institute of Technology Hyderabad, Telangana, India – 502285. *E-mail: atuldeshpande@iith.ac.in.
[b] Department of Chemistry, Indian Institute of Technology Hyderabad, Telangana, India – 502285.

† Electronic Supplementary Information (ESI) available: Characterization data - FTIR, XRD, FESEM, XPS, Raman, UV-Vis spectrum, DSC, Cyclic voltammogram, Voltage profiles and Impedance studies. See DOI: 10.1039/x0xx00000x

View Article Online
DOI: 10.1039/C8DT01787E




growth method, direct pyrolysis of nitrogen containing precursor and carbonization of polymers using inorganic/organic templates[23] are well known approaches for N-CNS synthesis. Among these, direct pyrolysis of precursor method is more attractive approach due to availability of various nitrogen contained precursors and ease of processing. Numerous nitrogen containing materials have been used as precursors including, ionic liquids (ILs), polymers and bio-mass.[23-25] Finding low cost and abundant nitrogen contained carbon precursor and optimization of carbonization temperature are the most important factors in direct pyrolysis of precursor method. Considering these aspects, we present, the use of ethyl cyanoacrylate as a unique precursor for the synthesis of nanocrystalline nitrogen doped graphene-like carbon nanosheets (N-CNS). This is a catalyst-free process, which involves polymerization of ethyl cyanoacrylate in aqueous NaCl solution, followed by carbonization in the presence of salt. Interestingly, during the heat treatment process, polymer precursor undergoes structural transformations similar to that seen in case degradation of polyacrylonitrile (PAN) which involve de-esterification and cyclization process, resulting in highly graphitic nitrogen doped carbon nanosheets. Carbon anode materials like N-CNS have the potential to deliver stable and high capacity for large number of cycles compared to other anodes like Si, $SnO_2$, and TiO2 etc. Graphite has the theoretical capacity of 372 mAh $g^{-1}$ with excellent cyclability. However, there is a need of higher energy and power density carbon to meet the present requirements like electric vehicles and smart grids. N-CNS can be one of the efficient contenders with reported capacity as high as 1865 mAh $g^{-1}$ and provide stable and high energy density compared to graphite.[24] In general, introducing heteroatoms like nitrogen can increase the number of active sites and can modulate their electronic and chemical properties. Thus N-CNS has high electronic conductivity, surface area and good electrochemical stability. These properties of N-CNS make them suitable candidates to be used as anode in lithium-ion batteries. Apart from N-CNS, other nitrogen doped nanostructured materials have also shown promising prospects as anode materials for Li-ion batteries (LIBs). N-doped carbon nanofibers have shown favorable capacity of 637 mAh $g^{-1}$ (at 2 A/g current density).[26] Hierarchical porous N-doped carbon nanosheets derived from silk[24] also show excellent capacity of ~1865 mAh $g^{-1}$ at 0.1 A $g^{-1}$. Owing to its potential application in commercial LIB's, it should be produced in bulk with safe and cost effective strategies. Here, we present a simple method of synthesizing the N-CNS using a household precursor via a simple, cost effective and high yield process.

## Experimental

### Materials

Commercially available ethyl cyanoacrylate (ECA) based Fevi kwik® glue (super glue) (product no: CPFK0.5PP213C-B, Pedilite, India) was used as a carbon precursor. Sodium chloride (NaCl) was obtained from RANKEM India (Analytical reagent grade), and deionized (DI) water of having resistivity of 18.2 MΩ cm was used for preparations of solutions.

### Synthesis

For the synthesis of nitrogen doped carbon nanosheets, the weight ratio of ethyl cyanoacrylate (Fevi kwik®) and NaCl (solution in DI water) was kept fixed at 1:2 for all samples. A saturated solution of NaCl was prepared by dissolving 33 g NaCl in DI water (approximately 92 ml). The saturated solution of NaCl was added rapidly to 16.5 g cyanoacrylate glue under vigorous stirring. Upon addition, the precursor underwent rapid exothermic polymerization, resulting in a whitish hard solid mixture of polyethyl cyanoacrylate and sodium chloride (PECA-NaCl). The resultant mixture was left undisturbed for 24 hours. Next, the excess of NaCl solution was drained off and the hard PECA-NaCl mass was dried at 80 °C for 12 hours. The resultant material was then ground to a fine powder. The sample obtained at this stage was labeled as, "as-dried sample" (PECA-NaCl). The powdered samples were carbonized in tubular furnace at 600 °C, 800 °C and 1000 °C under flowing Argon with a heating rate of 10 °C/min and 1 hour holding time. Finally, the carbonized powders were washed thoroughly with DI to remove NaCl, in order to get nitrogen doped carbon nanosheets. The resultant samples were labeled as N-CNS-600, N-CNS-800 and N-CNS-1000, respectively. Additionally, to understand the role of NaCl in carbon nanosheet formation, we prepared a carbon sample following the same protocol as that of N-CNS-1000 sample. However, instead of saturated aqueous solution NaCl, we use DI water as an initiator. This sample was denoted as CA-1000.

### Characterization

Crystallinity of as-dried and carbonized samples was assessed by X-ray diffraction (XRD) technique, using PANalytical (X'pert PRO) X-ray diffractometer, equipped with Cu – $k_\alpha$ radiation (wavelength, λ= 1.54 Å) source. To know more about the crystallinity and defect density, Raman spectra of samples carbonized at various temperatures were obtained using Bruker (SENTERRA) micro Raman spectrometer with the excitation laser source of wavelength 532 nm. High resolution transmission electron microscopy (HRTEM) (JEOL JEM 2100) (operated at 200 kV) and field emission scanning electron microscopy (FESEM) (Carle Zeiss SUPRA 40™) (operated at 20 kV) were used for morphological studies. Carbonized samples were prepared for HRTEM analysis by ultrasonicating the powdered samples in ethanol, followed by drop casting of resultant suspension on to the carbon coated copper grid. Fourier transform infra-red spectroscopy (FTIR) (Bruker TENSOR 37) studies were carried out to get insight into mechanism of decomposition of polymeric precursor. For this, the as-dried PECA-NaCl powdered samples were heat treated at 160 °C, 300 °C and 400 °C under flowing Argon for 1h with a heating rate of 10 °C/min. For FTIR studies, the as-dried samples and samples heat treated at different temperatures were mixed with KBr crystals, ground to a fine powder and pressed into a pellet using pelletizer and FTIR spectra were collected in transmission mode. To further examine the chemical content and bonding states, X-ray photoelectron

View Article Online
DOI: 10.1039/C8DT01787E




spectroscopic (XPS) studies were conducted using ESCA - Omicron XPS (System with Mg Kα as excitation source). UV Visible spectra of samples were obtained using PerkinElmer, Lambda 1050 UV/Vis/NIR spectrophotometer. For UV spectroscopy, the samples were prepared by dispersing carbonized powders in DI water (0.5 mg/25 ml of DI) using ultrasonicator. Thermal analysis of solid PECA-NaCl mixture was carried by differential scanning calorimetry (DSC) (DSC 404 F3, Netzsch). DSC analysis of as-dried PECA-NaCl sample was done under Argon atmosphere, with scan temperature range from room temperature to 1000 °C and 10 °C/min heating rate. BET surface area measurement of carbonized samples was carried with Quantachrome® ASiQwin™ (degassing at 300 °C for 4 hrs). The electrochemical measurement of the electrode comprising N-CNS-1000 powder as active mass was evaluated using Swagelok cells with a polyethylene-polypropylene trilayer separator (Celgard, Inc., Canada). The composite electrode comprised slurry of 90% active material, 10% PVDF (Kynar, Japan) in N methyl pyrollidone (Aldrich), were coated on to copper foil (>99.9%, Strem chemicals, Inc, US) current collector using doctor blade technique. The composite electrodes were dried under vacuum at 90 °C followed punched into 1cm diameter electrodes. The active masses of the electrodes are about 5 mg $cm^{-2}$. Li foils (Alfa Aesar) were used as counter electrodes. The electrolyte solution used is 1M $LiPF_6$ in 1:1 mixture of EC and DMC (Merck). Cyclic voltammetric study and Galvanostatic charge–discharge cycling was carried out using a multichannel battery tester (Arbin BT2000 - Battery Test Equipment, USA) within the operating voltage range of 2.5 to 0.01 V at various rates The impedance measurements were carried out in a frequency range between 1 MHz and 10 mHz in fully discharged condition (SoC 0) after 40 cycles at 2.3 V (2 h rest after charging to 3 V).

## Results and Discussion

Structural and functional properties of carbon based materials, especially nitrogen doped carbons, are profoundly affected by the choice of carbon precursors and the methods of preparation.[27,28] In particular, the properties of nitrogen containing carbon precursor such as their primary structure, molecular weight and degradation mechanism has been shown to influences the morphology, crystal phase evolution and extent of doping in resultant carbon materials. After careful consideration of these points, we selected ethyl cyanoacrylate as a carbon precursor. Commercial superglues which contain ~99.5% pure ethyl cyanoacrylate monomers are readily available. The monomer unit contains nitrile group which makes it a suitable precursor for the synthesis of N-doped carbons via direct synthesis approach.[29] Ethyl cyanoacrylate can be readily polymerized by variety of initiators including neutral, anionic and radical initiators. Polymerization of alkyl cyanoacrylates has been studied in detail and reports show that, the choice of initiator dictates polymerization rate, molecular weight, degradation and most importantly morphology.[30,31] Considering this, we selected NaCl as an initiator for polymerization of ethyl cyanoacrylate due to its low cost, non-toxic nature and chemical stability at high temperature. As the yield of polymer via vapor phase polymerization process tends to be very low, we decided to carry out the polymerization reaction in aqueous medium to improve the polymer yield. Though $Cl^-$ ions are stronger nucleophiles as compared to $H_2O$, both species can initiate polymerization of ethyl cyanoacrylate in aqueous medium. Therefore, saturated solution of NaCl was used in order to maintain high effective concentration of $Cl^-$ ions. During the synthesis process, the liquid monomer was mixed rapidly with saturated NaCl solution, which resulted in rapid polymerization of monomer. Polymerization was followed by aging, decantation of NaCl solution and drying process. The as-dried polymer was characterized by FTIR spectroscopy, XRD and SEM analysis. FTIR spectrum of as-dried PECA (Poly ethyl cyanoacrylate)-NaCl sample (**Fig. S1a)** shows all the characteristic IR active vibrational modes of PECA reported in the literature.[31,32,33] No peaks corresponding to ECA monomer were seen, which confirms that the sample is completely polymerized.

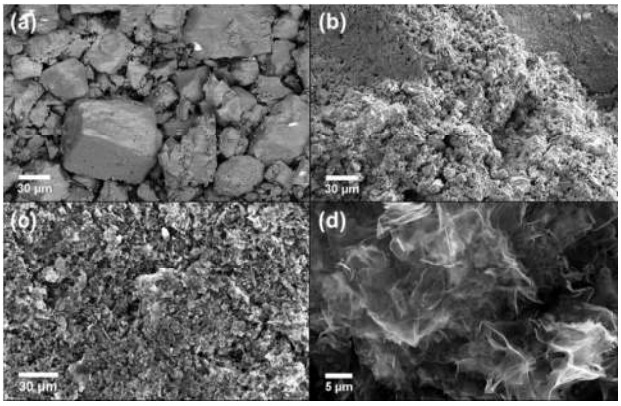


**Fig. 1** FESEM images of (a) as-dried sample (PECA-NaCl) (b) sample carbonized at 1000°C/ 1h in flowing argon gas and (c) low magnification and (d) intermediate magnification images of carbonized samples after washing with DI water (N-CNS-1000) which show that washing with DI water leads to removal of NaCl leaving behind carbon nanosheets organized in sponge-like morphology.

Crystallinity of as-dried sample was assessed by powder XRD. The XRD pattern of as-dried polymer (Fig. **S1b)** shows high intensity, sharp reflections corresponding to standard NaCl pattern (JCPDS No: 050628). Absence of any other reflections points out that PECA is in amorphous form. Furthermore, presence of NaCl reflections indicates that, though all the NaCl solution was decanted before the drying process, some NaCl got incorporated within polymer matrix. This may be due to retention of NaCl solution within the polymer network followed by recrystallization of NaCl crystals during the drying process. Homogeneous incorporation of NaCl with polymer matrix was further evident from scanning electron microscopy (SEM). Low magnification SEM images of as-dried sample (**Fig. 1a**) show particles having broad size distribution ranging from sub-micron sized particles to 100 µm sized particles. The as-dried samples were carbonized at 1000 °C in argon atmosphere. Since the melting point of NaCl is 801 °C, at the carbonization temperature (1000 °C) NaCl is present in molten form and recrystallizes from the melt upon cooling. **Fig. 1b** shows the morphology of sample after carbonization.

View Article Online
DOI: 10.1039/C8DT01787E




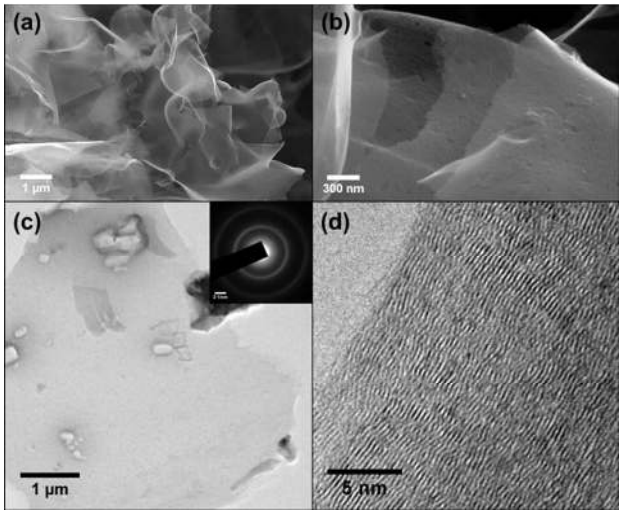


**Fig. 2** FESEM of N-CNS-1000 at (a) intermediate magnification image showing wrinkled carbon nanosheets and (b) and higher magnification showing surface porosity. HRTEM images of N-CNS-1000 at (c) low magnification indicating well defined pores. SAED pattern (Inset) shows ring pattern (002) and (101) reflections corresponding to polycrystalline graphitic phase (d) High magnification image of carbon nanosheets showing lattice fringes with regular periodic spacing.

Compared to as-dried samples, particle size reduced to less than few microns and very few larger particles were seen.

After carbonization, the samples were washed to remove NaCl. The SEM image of washed samples (N-CNS-1000) (**Fig. 1c**) shows that removal of NaCl leads to sponge-like porous structure. The intermediate magnification image of this sample (**Fig. 1d**), reveals that the sponge-like structures consist of aggregates of graphene-like wrinkled carbon sheets. At higher magnification (**Fig. 2a, b**), we see that the surface of these thin sheets is flecked with pore of sizes smaller than 50 nm. Such pores may result due to shrinkage which place during decomposition and crystallization process during the transformation of PECA to carbon nanosheets. It is well known that substitution of nitrogen atoms in place of carbon atoms in graphene leads to topological defects in graphene.[34,35] Thus, the smaller pores and the wrinkling effect can be attributed to nitrogen doping of carbon sheets. Occasionally, larger rectangular pores are also seen. These pores are clear indication that, the NaCl crystals are embedded within the carbon matrix and which are removed during washing process leaving behind well-defined pores. The as-dried samples were also carbonized at temperatures below the melting point of NaCl (600-800 °C). SEM images of these samples (N-CNS-600 and N-CNS-800) (**Fig. S2**) show the distinct carbon nanosheet morphology similar to 1000 °C carbonized samples. This indicates that NaCl in molten state is not necessary for the formation of carbon nanosheets. The thickness of N-CNS-600, N-CNS-800 and N-CNS-1000 samples was found to be 6.33 ± 0.9 nm, 6.16 ± 1.0 nm and 6.23 ± 1.0 nm, respectively (based on 50 measurements per sample). This indicates that carbonization temperature has very little effect on the thickness of carbon nanosheets. The transmission electron microscopy (TEM) images of carbonized samples are consistent with the FESEM results, the low magnification image (**Fig. 2c**)

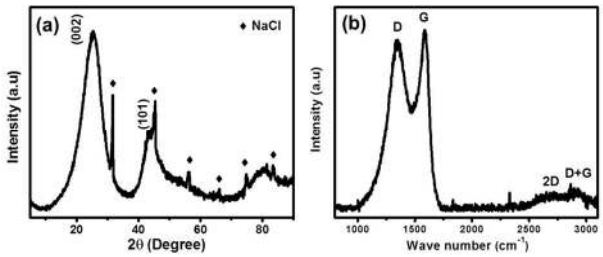


**Fig. 3** (a) XRD pattern of N-CNS-1000 sample showing broad reflections corresponding to graphitic carbon along with sharp reflections corresponding to NaCl and (b) Raman spectrum of N-CNS-1000.

shows wide sheets having dimensions in the range 5-10 µm. Well defined rectangular pores generated due to the removal of trapped NaCl crystals in the nanosheets are clearly seen along with smaller pores. The selected area electron diffraction (SAED) pattern (**Fig. 2c** inset) shows a diffused ring pattern which indicates that the carbon nanosheets are nanocrystalline in nature. The higher magnification HRTEM images of N-CNS-1000 (see **Fig. 2d**) taken from the edge part reveals the distinct layered stacking with short range ordering (buckled structure) The interlayer spacing was found to be 0.34 ± 0.03 nm (based on 250 measurements), which is slightly larger than the interlayer distance of graphitic carbon (0.335 nm).[8] The increased d-spacing might be attributed to the topological defects induced due to nitrogen doping.

Though HRTEM results show that N-CNS-1000 samples exhibit good crystallinity, the information obtained is restricted to locally observed morphology and crystallinity, for a small amount of sample. On the other hand, XRD technique gives information on long range ordering over large sample volume. Thus to assess the crystallinity of the bulk of sample, XRD studies of N-CNS-1000 were carried out. The XRD pattern of N-CNS-1000 sample (**Fig. 3a**) shows reflections centered at 25.33° and 43.12 that can be ascribed to the (002) and (101) reflections of graphitic carbon, respectively.[36] The broad nature of the reflection corresponding to carbon indicates that N-CNS-1000 sample is nanocrystalline in nature. The interlayer distance "d" of (002) plane obtained using Bragg's law, is ~ 0.35 nm which is larger than the d-spacing of standard graphite and is in agreement with HRTEM results (lattice spacing ~ 0.34 nm). The literature reports show similar increase in d-spacing in case of few layer graphene materials.[37] It has also been reported in case nitrogen doped carbons that, lattice parameter increases due to substitution of carbon atoms with nitrogen atoms in carbon framework. Nitrogen doping also results in introduction of defects in carbon framework which leads to increase in d-spacing.[38,39] Additionally, sharp reflections corresponding to NaCl were also seen in XRD pattern of N-CNS-1000 sample, which indicates that, even after thorough washing, NaCl still remains within carbon nanosheets matrix. This shows that, small amount NaCl crystals may be trapped within tightly folded carbon nanosheet, which makes it difficult to eliminate them completely by washing.

View Article Online
DOI: 10.1039/C8DT01787E




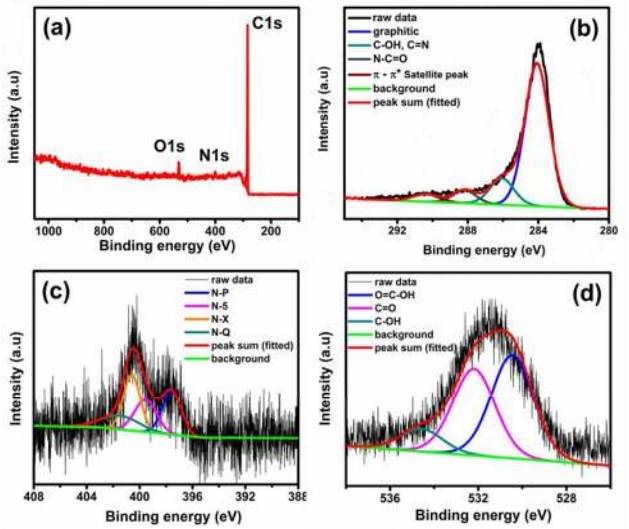


**Fig. 4** Survey scanned XPS spectrum (a) and fine scanned spectra of Cs1s (b), N1s (c) and O1s (d) of N-CNS-1000.

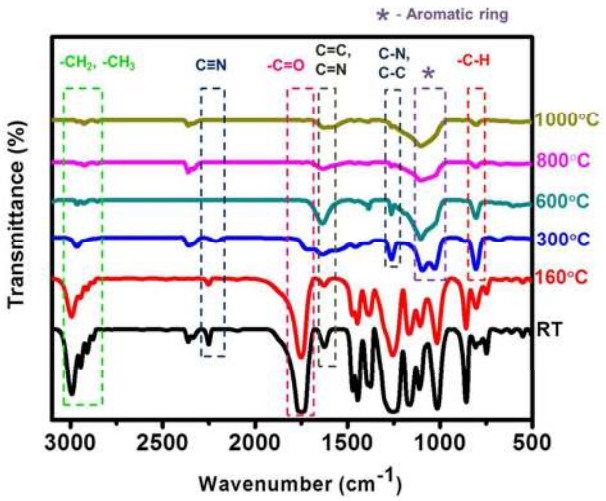


**Fig. 5** FTIR spectra of PECA-NaCl sample, carbonized at various temperatures.

Raman spectrum of graphene-like nitrogen doped carbon nanosheets (N-CNS-1000) (shown in **Fig. 3b**) shows two major bands positioned at 1580 $cm^{-1}$ and 1350 $cm^{-1}$. These bands correspond to G-band and D-band respectively of graphitic carbon with the $I_D/I_G$ ratio of 0.93. The shift in the peak position of G-band towards to higher frequency is an indication for existence of nanocrystalline domains, i.e. smaller in-plane $sp^2$ domains.[40-43] In addition to nanocrystalline nature, nitrogen doped carbons also show blue shift in peak position of G-band. Nitrogen doping also leads to generation of topological defects which results in increase in D band intensity.[40] Apart from D and G bands three broad and low intensity bands in the range of 2600-3200 $cm^{-1}$ are also seen in Raman spectrum of N-CNS-1000 sample (**Fig. 3b**). These bands can be ascribed to 2D (2710$cm^{-1}$) and D" (3200 $cm^{-1}$) bands and defect related D + G band (2920 $cm^{-1}$). These bands are characteristic of $sp^2$ graphitic carbons. Reports show that, reduction in crystallite size, doping and structural defects for graphitic carbon result in reduction in peak intensity and peak broadening of 2D peaks as seen in case of N-CNS-1000 sample.[41] Similar Raman spectra were observed in case of N-CNS-600 and N-CNS-800 (see **Fig. S4**) with $I_D/I_G$ ratios of 0.67 and 0.88, respectively. As the carbonization temperature is increased, more number of nitrogen atoms are eliminated from the hexagonal network, which leads to introduction of additional defects in carbon network and increase in porosity. Thus, higher carbonization temperature leads to higher $I_D/I_G$ for N-CNS-1000 ($I_D/I_G$ = 0.93) as compared N-CNS-600 and N-CNS-800 samples. Increase in the intensity of 2D band from N-CNS-600 to N-CNS-1000 also indicates enhanced graphitization with increase in carbonization temperature. Additionally, UV-Vis spectrum of N-CNS-1000 (see in **Fig. S5**) shows sharp absorption peak around 265 $cm^{-1}$ which is attributed to the π-π* transition of carbon-carbon double bonds. This spectrum is consistent with absorption range of graphene and graphene-like carbon nanomaterials and it is a clear evidence for the formation of graphene-like carbon nanosheets.[44] Thus, based on above discussion, it is clear that Raman and UV-Vis spectroscopy results are consistence with the HRTEM and XRD results, confirming the nanocrystalline, graphitic nature in N-CNS and nitrogen doping induced defect structure.

To further assess the elemental composition of carbon nanosheets, nature of bonding and structural evolution, XPS studies were conducted on samples carbonized at 600 °C, 800 °C and 1000 °C. **Fig. 4a** shows, full scan XPS spectrum of N-CNS-1000 sample with three characteristic peaks at 284 eV, 401 eV and 532 eV that correspond to C1s, N1s and O1s, respectively.[45,46] The amount of carbon, nitrogen and oxygen in N-CNS-1000 are 93.23%, 2.67% and 4.13%, respectively. The deconvoluted C1s spectrum of carbon nanosheets (**Fig. 4b**) shows well fitted peaks around 284 eV, 286 eV, 288 eV and 290 eV which belong to C=C ($sp^2$ C), C=N, N-C=O and π-π* satellite peak which is a signature peak for graphitic $sp^2$ C, respectively. Thus it is evident from C1s spectrum of N-CNS-1000 sample that carbon exists in the graphitic form. The fine scan N1s spectrum of N-CNS-1000 (**Fig. 4c**) shows presence of $sp^2$ nitrogen containing functional groups such as pyridinic-N (N-P) (~ 397 eV), pyrrolic-N (N-5) (~399 eV), pyridonic -N (N-X) (~ 400 eV) and quaternary-N (N-Q) (~ 401 eV). All these groups have nitrogen as a part of 5 or 6 membered rings, which shows that nitrogen atoms are located within the graphitic carbon network. Typically, nitrogen in, N-5, N-X, N-6 form is responsible for creation of structural defects i.e. pores in hexagonal network of carbon.[46] Introduction of pores within carbon framework lead to increase in the number of unsaturated carbon atoms placed at edge positions. These unsaturated carbon atoms are prone to oxidation when exposed to atmospheric oxygen.[47] Consequently, we see peaks corresponding to oxygen functional groups for sample carbonized at 1000 °C. **Fig. 4d** shows the O1s spectrum of N-CNS-1000 sample with peaks at 530 eV, 532 eV and 534 eV which belong to O=C-OH, C=O and C-OH, respectively. The chemical and structural changes are reflected in BET surface area values of N-CNS-600, N-CNS-800 and N-CNS-1000 are 73

View Article Online
DOI: 10.1039/C8DT01787E


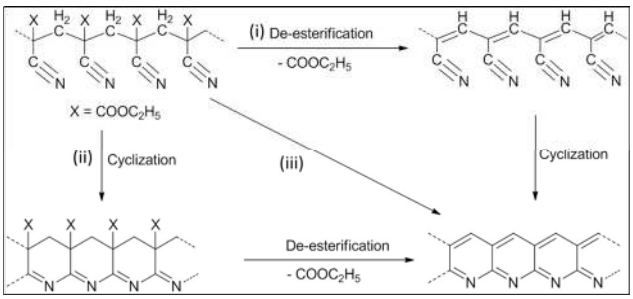


**Scheme 1.** Possible mechanism for ladder structure formation during heat treatment (< 600°C) of poly ethyl cyanoacrylate under inert atmosphere.

$m^2 g^{-1}$, 59 $m^2 g^{-1}$ and 169 $m^2 g^{-1}$, respectively. Slight decrease in surface area from N-CNS-600 to N-CNS-800 is due to increase in graphitization. Whereas as large increase in surface area of N-CNS-1000 can be attributed to the loss of nitrogen and other functional groups.

In order to follow the structural evolution of carbon network with heat treatment temperature, the XPS data of samples carbonized at 600 °C (N-CNS-600) and 800 °C (N-CNS-800) was compared with sample carbonized at 1000 °C. **Fig. S6** provides fine scanned XPS spectra of C1s, N1s and O1s of samples calcined at different temperature. It can be seen that, with increase in carbonization temperature, there is notable increase in carbon content and decrease in oxygen content, whereas nitrogen content decreases only marginally (**Fig. S6**). Furthermore, N1s and C1s spectra of CNS samples carbonized at 600 °C and 800 °C (**Fig. S6**) show peaks corresponding to $sp^2$ nitrogen and $sp^2$ carbon containing functional groups similar to sample carbonized at 1000 °C. Absence of peaks corresponding to $sp^3$ nitrogen or $sp^3$ carbon clearly shows that even at low carbonization temperatures nitrogen containing carbon exists in the form of network similar to graphitic carbon structure.

In addition to XPS studies, FTIR also gives valuable insight into molecular structure of the materials. Therefore, FTIR studies were performed to understand the chemical transformation and structural changes happening during carbonization of as-dried precursor. In order to determine temperature points at which the sample undergoes decomposition/ structural transformation, Differential scanning calorimetry (DSC) of as-dried samples was done under Ar gas flow. The DSC analysis of as-dried sample (see **Fig. S8**) shows an endothermic reaction in the range of 150-300 °C with maximum heat absorption at 235 °C. Thereafter no significant heat flow was observed till 600 °C. Therefore, in order to analyze chemical changes during the decomposition we selected 160 °C, 300 °C, 600 °C, 800 °C and 1000 °C as the reference points for FTIR analysis. Comparison of FTIR spectra for as-dried and all the heat treated samples are shown in **Fig. 5**. It can be seen that the FTIR spectra of as-dried and sample heat treated at 160 °C are quite similar except for minor change in the intensity of characteristic peaks of PECA. This implies that, the polymeric precursor does not undergo any change in its chemical composition till 160°C. At 300 °C, the intensity of peaks corresponding to $–CH_2$, $-CH_3$ (2800-2990 $cm^{-1}$ for C-H stretch, 1000-1470 $cm^{-1}$ for C-H bending), C=O (1746 $cm^{-1}$) and C-O (1255 $cm^{-1}$) decreased drastically. This indicates that at 300 °C de-esterification i.e. the elimination of ester side of group ($-COOC_2H_5$) of PECA backbone takes place to a significant extent. Further we also see decrease in intensity of peak at 2250 $cm^{-1}$ which corresponds to C≡N group, however, the intensity of peak at 1620 $cm^{-1}$ (C=C, C=N) increases and new peak around 1261 $cm^{-1}$(C-N, C-C) appears. In addition, peaks at 1095 $cm^{-1}$, 1024 $cm^{-1}$and 805 $cm^{-1}$ (=C-H bending) which correspond to heteroatomic aromatic ring structure [48,49] also appear. These changes in FTIR spectra of 160 and 300 °C heat treated samples are very peculiar. Similar changes in FTIR spectra of polyacrylonitrile (PAN) fibers heat treated at similar temperature range were also observed.[33] Houtz, *et al.,* proposed that during decomposition of PAN the polymer chains undergo cyclization process which involves adjacent C≡N side group. During cyclization C≡N gets converted to C=N resulting in six membered pyridine like ring structure. Consequently, the aliphatic polymeric chains transform into cyclic "ladder polymer". In addition, reports show that during degradation of PAN fibers dehydrogenation reaction also takes place which stabilizes the polymer backbone through formation of double bonds.[50] By comparing our data with reports on PAN fiber decomposition studies, we believe that in thermal degradation of as-dried samples, PECA undergoes cyclization similar to that of PAN as evident from noticeable decrease in intensity of peak C≡N (2250 $cm^{-1}$), increase in intensity of peak of C=C/C=N (1620 $cm^{-1}$) and appearance of C-N peak (1260 $cm^{-1}$). Dehydrogenation process was also evident from appearance of 1620 $cm^{-1}$ (C=C), 1095 $cm^{-1}$ and 1024 $cm^{-1}$ peaks. The FTIR spectra of 600 °C heat treated sample shows that peaks for C=O and C≡N disappears completely, whereas peaks for C=C/C=N, C-N and peaks corresponding to heteroatomic aromatic ring structure become most prominent. This indicates that at 600 °C PECA undergoes de-esterification and cyclization process to a larger extent. As discussed earlier, N1s XPS spectrum of 600 °C shows that $sp^3$ nitrogen containing groups are absent and nitrogen exists only in the form of cyclic functional groups such as pyridinic-N (N-P) and pyrrolic-N (N-5). This further supports the evidence obtained from FTIR that cyclization process is complete by 600 °C. Furthermore, C1s spectrum of 600 °C sample (supporting information **Fig. S6**) shows that major fraction of carbon exists in C=C-H form (283.8 eV) along with C=C (284 eV) with very small fraction of C=O (288 eV) functional group. This indicates that the de-esterification process and dehydrogenation process also occurs to a great extent by 600 °C.

Thus, drawing parallel from degradation of PAN, a proposed mechanism is schematically shown in **Scheme 1**, which shows that formation of ladder structure may result in three possible ways (i) de-esterification followed by cyclization, (ii) cyclization followed by de-esterification and (iii) simultaneous de-esterification and cyclization. Reports show that in case of PAN, sequence of cyclization and dehydrogenation process depends on the heat treatment environment conditions i.e. oxidative, reductive or neutral gas environment.[51] Based on the FTIR and XPS studies we anticipate that, for the heat treatment protocol we followed,

View Article Online
DOI: 10.1039/C8DT01787E


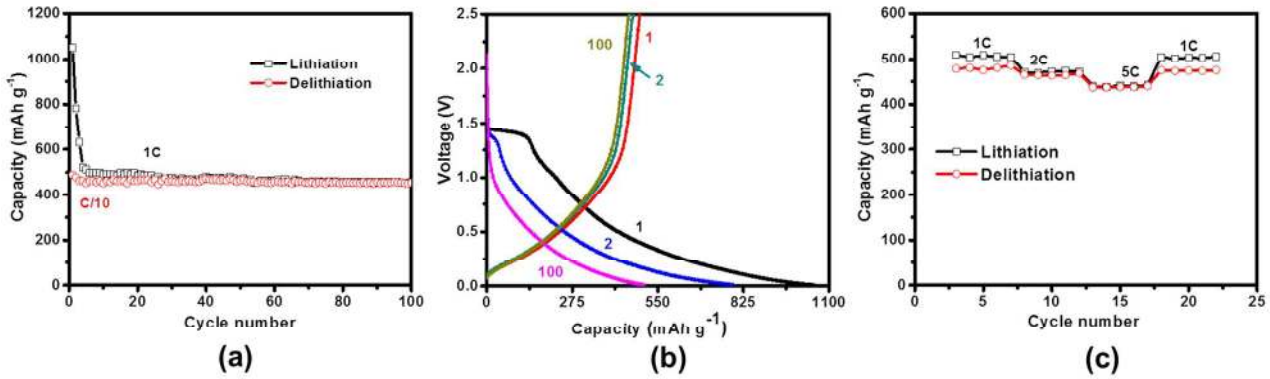


**Fig. 6** (a) Capacity vs. cycle number plot for the N-CNS composite electrodes. Initial 2 cycles at C/10 rate, followed by charge-discharge at 1C rate for 100 cycles; (b) Lithiation and delithiation voltage profiles for the N-CNS composite electrodes during 1, 2 and 100$^{th}$ cycles; (c) C rate performance for the N-CNS composite electrode at 1C, 2C and 5C rate (as indicated) during 22 cycles at 25$^{o}$C. Initial 2 cycles are not presented here.

the ladder structure formation might be taking place by simultaneous de-esterification and cyclization process. Comparison of FTIR spectra of 600 °C, 800°C and 1000 °C shows that intensity of C=N/ C=C (1620 cm$^{-1}$) and C-N (1261 cm$^{-1}$) decreases which indicates elimination of nitrogen from the sample which is consistent with reduction in atomic percentage of nitrogen as obtained from analysis of N1s XPS spectra of these samples (**Fig. S7**). Similar reduction in nitrogen content was also observed in case of carbonization of PAN fibers, where the reduction in nitrogen content is attributed to elimination of nitrogen during crosslinking between ladder structures to yield graphite-like layered structure.[51] Additionally, the intensity of =C-H (805 cm$^{-1}$) also decreases from 600-1000 °C which is consistent with reduction in contribution from C=C-H peak (283.8 eV) seen in C1s XPS spectra of these samples.[52] In summary, FTIR data along supported with XPS results shows that during the heat treatment in inert atmosphere till 1000 °C, polymer precursor undergoes concurrently through cyclization and de-esterification, followed by formation of graphite-like layered structure and finally resulting in formation of nitrogen doped graphene-like carbon nanosheets.

Cyclic-Voltammetric study of N-CNS-1000 was carried out to assess the redox behaviour of nitrogen-doped carbon nanosheets (**Fig. S9**). The broad reduction peak starting from 0.8 V to 0.36 V corresponds to the formation of solid electrolyte interphase (SEI) and the peak vanishes in the successive cycles. The peak close to 0 V corresponds to Li-intercalation in carbon anodes. The difference in the area of two curves is equivalent to irreversible capacity or capacity loss in 2$^{nd}$ cycle which is due to the formation of SEI in the 1$^{st}$ cycle where lot of Li-ions are consumed. Based on the CV studies, the electrochemical behavior of N-CNS-1000 as anode in lithium batteries were assessed by constant current charge-discharge cycling in the voltage range from 2.5 V to 0.01 V at various C rates as shown in **Fig. 6**. These cells show excellent cyclability of > 480 mAh g$^{-1}$ at 1C rate as shown in **Fig. 6a**. The charge-discharge voltage profiles of N-CNS composite anode in the 1$^{st}$, 2$^{nd}$ and 100$^{th}$ cycle are shown in **Fig. 6b**. N-CNS composite anodes deliver an initial discharge capacity of 1052 mAh g$^{-1}$ and a reversible capacity of 480 mAh g$^{-1}$ during charging. High irreversible capacity is due to formation of SEI layer during the first cycle. The synthesis method helps in the formation of the N-CNS with highly folded morphology (**Fig. 2a**) and more curled edges which generate lot of cavities. These cavities may act as reservoirs for accommodating high lithium content which is responsible for high capacity of N-CNS. N-CNS-1000 shows excellent cycling stability with the average capacity of 480 mAh g$^{-1}$. There is a flat plateau in the first discharge profile in **Fig. 6b** which may be due to the interaction of Li-ion with chloride ion of trace amount of NaCl which is trapped in the N-CNS (during synthesis) and is not removed while washing N-CNS with water. The plateau almost disappeared during 2$^{nd}$ cycle indicates the irreversibility of LiCl. **Fig. 6c** shows the galvanostatic charge-discharge capacities at different rates. The **Fig. 6c** shows the average reversible capacity of 480 mAh g$^{-1}$ can be obtained at 1C rate, and even the cells deliver an excellent capacity of 460 mAh g$^{-1}$ at 2C and 440 mAh g$^{-1}$ at 5C rate. From the foregoing discussion it is clear that N-CNS synthesized by polymerization of Fevi kwik® shows excellent electrochemical performance than that of graphite.

For comparison, the electrochemical performance of N-CNS-800, N-CNS-600 and CA-1000 was also carried out. It can be clearly observed from the **Fig.S10**, that N-doped graphene-like carbon nano-sheets calcined at 1000 $^{o}$C (N-CNS-1000) shows improved electrochemical performance compared to the corresponding sample calcined at 800 $^{o}$C (N-CNS-800) and 600 $^{o}$C (N-CNS-600). It is also observed that 800 $^{o}$C calcined material shows 12% improvement in electrochemical performance than 600 $^{o}$C calcined material. The sample prepared without NaCl and carbonized at 1000 $^{o}$C (CA-1000) shows reasonably high initial discharge capacity (662 mAh g$^{-1}$at 0.1C) and charge capacity (456 mAh g$^{-1}$ at 0.1C), however, the initial cycle performance of CA-1000 samples is still less compared to N-CNS-1000 sample. Further, CA-1000 shows rapid capacity fading with successive cycles. The improved electrochemical performance is attributed to better graphitization observed for N-CNS-1000 compared to all the other samples. Additionally, presence of pores formed by highly folded morphology and more curled edges. It is also

View Article Online
DOI: 10.1039/C8DT01787E




observed that on increasing the carbonization temperature the porosity of the material increases which is responsible for the improvement in electrochemical performance of 1000 $^{o}$C calcined material compared to 800 $^{o}$C and 600 $^{o}$C calcined sample. Whereas the sample without NaCl which is devoid of nanostructured features , shows less graphitization and lacks the voids and pores which makes complex path for the Li-ion de/intercalation due to which there is rapid capacity fade.

The lithium ion battery performance also depends on the internal resistance of the cell which in turn depends on nature of the electrode material and stable SEI layer formation. To assess the internal conductivity, electrochemical impedance studies were carried out 40 cycles. Impedance is the indirect way of expressing the conductivity. N-doped graphene-like carbon nano-sheets carbonized with NaCl at 1000 $^{o}$C (N-CNS-1000) showed low ohomic (6.9 ohm.cm$^2$) and charge transfer resistance ($R_{ct}$ - 109 ohm.cm$^2$) compared to material carbonized at 800 $^{o}$C ($R_{ct}$ – 135 ohm.cm$^2$) and 600 $^{o}$C ($R_{ct}$ – 152.52 ohm.cm$^2$). Whereas the material carbonized without NaCl is (CA-1000) showed high charge transfer ($R_{ct}$ – 155 ohm.cm$^2$). The low charge transfer resistance of material calcined with NaCl is attributed to the formation of more ordered structure due to presence of NaCl. The above observation suggest that the N-CNS-1000 improved conductivity compared to N-CNS-600, N-CNS-800 and CA-1000.

Apart from acting as an initiator we wanted to understand if NaCl plays any role in the formation of carbon nanosheets. Therefore, we carried out the polymerization of ethyl cyanoacrylate in the absence of NaCl i.e. we used DI water rather than saturated aqueous solution of NaCl for the polymerization process. The polymeric material upon carbonization (CA-1000) did not show nanosheet like morphology (see **Fig. S3**). Additionally, High resolution transmission electron microscopy studies of this carbonized sample revealed (Fig. S3c) lack of long range ordering. However, nano sized domains with short range order with interlayer spacing of d ≈ 0.38 ± 0.05 nm (based on 250 measurements) were observed. These features of bulk carbon sample are similar to the turbostratic carbon but dissimilar from the carbon nanosheets (N-CNS) prepared through salt mediated process. So it is clear that NaCl does play a role in the formation of carbon nanosheets. Throughout the study, we also saw indications that NaCl may be acting as structure directing agent in the formation of carbon nanosheets. For example, rectangular nanopores in carbon nanosheets as observed in SEM and TEM images suggest that presence NaCl crystals in polymerized samples may not be merely due to recrystallization from trapped solution during drying process. Liu *et al.*[53] used a deep eutectic salt composition of LiCl/KCl with low melting point. They state that molten salt acts as a "solvent" which allows dissolution and precipitation of carbon in the form of nanosheets. However, in our case, SEM images of samples carbonized at 600 °C and 800 °C (N-CNS-600 and N-CNS-800) (**Fig. S2**) show distinct carbon nanosheet morphology similar to 1000 °C. This means that NaCl in molten state is not necessary for the formation of carbon nanosheets. Other literature reports which used NaCl as template for carbon nanosheets show that, NaCl acts as a hard template for deposition of precursor material which converts to thick carbon nanosheets upon carbonization below melting point of NaCl.[54] In our case, if NaCl crystals were acting as a hard template, we should see distinct difference in the morphology of samples carbonized below and above melting point of NaCl. However, we do not see such differences. Hence, we believe that NaCl does not act as a passive template in our case. Thus based on the current results, the exact role in the formation of carbon nanosheets is still obscure. We are carrying out further studies to know the exact role of NaCl and mechanism of formation of carbon nanosheets.

## Conclusion

To summarize, we presented use of commercially available ethyl cyanoacrylate based super glue as a unique precursor for the synthesis of nanocrystalline nitrogen doped graphene-like carbon nanosheets (N-CNS). This catalyst-free process involved polymerization of ethyl cyanoacrylate in aqueous NaCl solution, followed by carbonization of resultant polymeric mass in the presence of salt at 1000°C. Detailed spectroscopic analysis of the degradation products of polymeric precursor at various heat treatment temperatures in inert atmosphere reveals that, polymer precursor undergoes structural transformations similar to that seen in case degradation of polyacrylonitrile (PAN) involving de-esterification and cyclization process. The result of this peculiar degradation behavior is, nanocrystalline, graphitic, nitrogen doped carbon nanosheets. N-CNS used as anodes for lithium battery showed stable reversible capacities of 480 mAh g$^{-1}$ (1C rate) for 100 cycles. These results indicate that N-CNS could be used as a promising anode material for next generation lithium ion batteries. We believe that, unique way in which PECA undergoes structural transformation during carbonization can be useful to design new nanostructured graphitic carbons for a wide range of other applications including energy storage, sensors and catalysis.

## Conflicts of interest

The authors declare no conflict of interest.

## Acknowledgements

We are grateful Dr. Srinivasan Anandan (Senior Scientist, ARCI, Hyderabad, India) for carrying out XPS spectroscopic studies of carbon samples. We thank IIT Hyderabad and MHRD for financial support.

## Notes and references

1 J. Jortner and C. N. R. Rao, *Pure Appl. Chem.*, 2002, **74**, 1491-1506.
2 F. Zaera, *Chem. Soc. Rev.*, 2013, **42**, 2746-2762.

View Article Online
DOI: 10.1039/C8DT01787E





3 A. S. Arico, P. Bruce, B. Scrosati, J.-M.Tarascon and W. V. Schalkwijk, *Nat. Mater*., 2005, **4**, 366-377.
4 S. Chen, G. He, H. Hu, S. Jin, Y. Zhou, Y. He, S. He, F. Zhao and H. Hou, *Energy Environ. Sci.*, 2013, **6**, 2435-2439.
5 Y. P. Wu, E. Rahm and R. Holze, *J. Power Sources*, 2003, **114**, 228-236.
6 X.-T. Chen, K.-X. Wang, Y.-B. Zhai, H.-J. Zhang, X.-Y. Wu, X. Weia and J.-S. Chen, *Dalton Trans.*, 2014, **43**, 3137-3143.
7 A. S. Bozzi, R. L. Lavall, T. E. Souza, M. C. Pereira, P. P. De Souza, H. A. De Abreu, A. De Oliveira, P. F. R. Ortega, R. Paniago and L. C. A. Oliveira, *Dalton Trans.*, 2015, **44**, 19956-19965.
8 M. J. Allen, V. C. Tung and R. B. Kaner, *Chem. Rev.*, 2010, **110**, 132-145.
9 X. Mao, G. C. Rutledge and T. A. Hatton, *Nano Today*, 2014, **9**, 405-432.
10 Y. Li, Q. Meng, S.-M. Zhu, Z.-H. Sun, H. Yang, Z.-X. Chen, C.-L. Zhu, Z.-P. Guo and Di Zhang, *Dalton Trans.*, 2015, **44**, 4594-4600.
11 E. W. Hill, A. Vijayaragahvan and K. Novoselov, *IEEE Sens. J*., 2011, **11**, 3161-3170.
12 A. K. Geim, *Science*, 2009, **324**, 1530-1534.
13 G. Qin, Z. Fang and C. Wang, *Dalton Trans.*, 2015, **44**, 5735-5745.
14 R.-H. Kim, M.-H. Bae, D. G. Kim, H. Cheng, B. H. Kim, D.-H. Kim, M. Li, J. Wu, F. Du, H. S. Kim, S. Kim, D. Estrada, S. W. Hong, Y. Huang, E. Pop and J. A. Rogers, *Nano Lett*., 2011, **11**, 3881-3886.
15 V. Singh, D. Joung, L. Zhai, S. Das, S. I. Khondaker and S. Seal, *Prog. Mat. Sci*., 2011**, 56**, 1178-1271.
16 A. A. Balandin, *Nat. Mater*., 2011, **10**, 569-581.
17 Y. Shao, J. Wang, H. Wu, J. Liu, I. A. Aksay and Y. Lin, *Electroanalysis*, 2010, **22**, 1027-1036.
18 H. Wang, Z. Xu, A. Kohandehghan, Z. Li, K. Cui, X. Tan, T. J. Stephenson, C. K. King'ondu, C. M. B. Holt, B. C. Olsen, J. K. Tak, D. Harfield, A. O. Anyia and D. Mitlin, *ACS Nano*, 2013, **7**, 5131-5141.
19 J. Duan, S. Chen, M. Jaroniec and S. Z. Qiao, *ACS Catal*., 2015, **5**, 5207-5234.
20 R. Lv, Q. Li, A. R. Botello-Mendez, T. Hayashi, B. Wang, A. Berkdemir, Q. Hao, A. L. Elias, R. Cruz-Silva, H. R. Gutierrez, Y. A. Kim, H. Muramatsu, J. Zhu, M. Endo, H. Terrones, J.-C. Charlier, M. Pan and M. Terrones, *Sci. Rep*., 2012, **2**, 586 (1-8).
21 X. Xie, D. Su, J. Zhang, S. Chen, A. K. Mondal and G. Wang, *Nanoscale*, 2015, 7, 3164-3172.
22 X. Xie, J. Long,J. Xu, L. Chen, Y. Wang, Z. Zhanga and X. Wang, *RSC Advances*, 2012, 2, 12438-12446.
23 H. Wang, T. Maiyalagan and X. Wang, *ACS Catal*., 2012, **2**, 781-794.
24 J. Hou, C. Cao, F. Idrees and X. Ma, *ACS Nano*, 2015, **9**, 2556-2564.
25 J. P. Paraknowitsch, J. Zhang, D. Su, A. Thomas and M. Antonietti, *Adv. Mater*., 2010, **22**, 87-92.
26 L. Qie, W.-M. Chen, Z.-H. Wang, Q.-G. Shao, X. Li, L.-X. Yuan, X.-L. Hu, W.-X. Zhang and Y.-H. Huang, *Adv. Mater*., 2012, **24**, 2047-2050.
27 Y. Deng, Y. Xie, K. Zou X. Ji, *J. Mater. Chem. A*, 2016, **4**, 1144-1173.
28 S. Yang, R. Bachman, X. Feng and K. Mullen, *Acc. Chem. Res*., 2013, **46**, 116-128.
29 Fevikwik GP, Materials Safety Data Sheet, Pidilite Industries Limited, Mumbai, 2011.
30 M. I. Frolova, L. A. Oshmarina, V. I. Chervyakova and E. G. Pomerantseva, *Polym. Sci*., 1991, **33**, 1939-1944.
31 P. J. Mankidy, R. Rajagopalan and H. C. Foley, *Polymer*, 2008, **49**, 2235-2242.
32 S. K. Tomlinson, O. R. Ghita, R. M. Hooper and K. E. Evans, *Vib. Spectrosc*., 2006, **40**, 133-141.
33 Z. Wangxi, L. Jie and W. Gang, *Carbon*, 2003, **41**, 2805-2812.
34 B. He, W.-C. Li and A.-H. Lu, *J. Mater. Chem. A*, 2015, **3**, 579-585.
35 K. Suenaga, M. Yudasaka, C. Colliex and S. Iijima, *Chem. Phys. Lett*., 2000, **316**, 365-372.
36 C. N. R. Rao, K. Kanishka Biswas, K. S. Subrahmanyam and A. Govindaraj, *J. Mater. Chem*., 2009, **19**, 2457-2469.
37 E. J. Yoo, J. Kim, E. Hosono, H.-S. Zhou, T. Kudo and I. Honma, *Nano Lett.* 2008, **8**, 2277-2282.
38 M. K. Rybarczyk, M. Lieder and M. Jablonska, *RSC ADVANCES* 2015, **5**, 44969-44977.
39 D. Geng, S. Yang, Y. Zhang, J. Yang, J. Liu, R. Li, T.-K. Sham, X. Sun, S. Ye and S. Knights, *Appl. Surf. Sci.* 2011, **257**, 9193-9198.
40 A. C. Ferrari, *Solid State Commun*., 2007, **143**, 47-57.
41 L. M. Malard, M. A. Pimenta, G. Dresselhaus and M. S. Dresselhaus, *Phys. Rep*., 2009, **473**, 51-87.
42 M. A. Pimenta, G. Dresselhaus, M. S. Dresselhaus, L. G. Cancado, A. Jorio and R. Saito, *Phys. Chem. Chem. Phys*., 2007, **9**, 1276-1291.
43 A. C. Ferrari and J. Robertson, *Phys. Rev. B*, 2000, **61**, 14095-14107.
44 X. Zhu, Q. Liu, X. Zhu, C. Li, M. Xu, and Y. Liang, *Int. J. Electrochem. Sci.*, 2012, **7**, 5172-5184.
45 P. Chen, L.-K. Wang, G. Wang, M.-R. Gao, J. Ge, W.-J. Yuan, Y.-H. Shen, A.-J. Xie and S.-H. Yu, *Energy Environ. Sci.*, 2014, **7**, 4095-4103.
46 I. Bertoti, M. Mohai and K. Laszlo, *Carbon*, 2015, **84**, 185-196.
47 Y. Shao, S. Zhang, M. H. Engelhard, G. Li, G. Shao, Y. Wang, J. Liu, I. A. Aksay and Y. Lin, *J. Mater. Chem*., 2010, **20**, 7491-7496.
48 R. Setnescu, S. Jipa, T. Setnescu, W. Kappel, S. Kobayashi and Z. Osawa, *Carbon*, 1999, **37**, 1-6.
49 D. Zhu, C. Xu, N. Nakura and M. Matsuo, *Carbon*, 2002, **40**, 363-373.
50 R. C. Houtz, *Text. Res. J*., 1950, **20**, 786-801.
51 M. S. A. Rahaman, A. F. Ismail and A. Mustafa, *Polym. Degrad. Stab*., 2007, **92**, 1421-1432.
52 Y. Yamada, Y. Suzuki, H. Yasuda, S. Uchizawa, K. Hirose-Takai, Y. Sato, K. Suenaga and S. Sato, *Carbon*, 2014, **75**, 81-94.
53 X. Liu, C. Giordano and M. Antonietti, *Small*, 2013, **10**, 193-200.
54 J. Zhang, H. Zhu, P. Wu, C. Ge, D. Sun, L. Xu, Y. Tanga and Y. Zhoua, *Nanoscale,* 2015, **7**, 18211-18217.

View Article Online
DOI: 10.1039/C8DT01787E



## Table of Contents

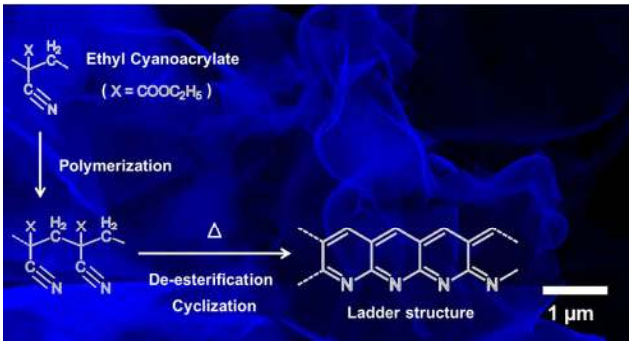


Morphology of nitrogen doped graphene-like carbon nanosheets along with proposed mechanism for ladder structure formation during carbonization of commercial glue.